Archival Report

Biological Psychiatry: CNNI

Cognitive Control Errors in Nonhuman Primates Resembling Those in Schizophrenia Reflect Opposing Effects of NMDA Receptor Blockade on Causal Interactions Between Cells and Circuits in Prefrontal and Parietal Cortices

Erich Kummerfeld, Sisi Ma, Rachael K. Blackman, Adele L. DeNicola, A. David Redish, Sophia Vinogradov, David A. Crowe, and Matthew V. Chafee

ABSTRACT

BACKGROUND: The causal biology underlying schizophrenia is not well understood, but it is likely to involve a malfunction in how neurons adjust synaptic connections in response to patterns of activity in networks. We examined statistical dependencies between neural signals at the cell, local circuit, and distributed network levels in prefrontal and parietal cortices of monkeys performing a variant of the AX continuous performance task paradigm. We then quantified changes in the pattern of neural interactions across levels of scale following NMDA receptor (NMDAR) blockade and related these changes to a pattern of cognitive control errors closely matching the performance of patients with schizophrenia.

METHODS: We recorded the spiking activity of 1762 neurons along with local field potentials at multiple electrode sites in prefrontal and parietal cortices concurrently, and we generated binary time series indicating the presence or absence of spikes in single neurons or local field potential power above or below a threshold. We then applied causal discovery analysis to the time series to detect statistical dependencies between the signals (causal interactions) and compared the pattern of these interactions before and after NMDAR blockade.

RESULTS: Global blockade of NMDAR produced distinctive and frequently opposite changes in neural interactions at the cell, local circuit, and network levels in prefrontal and parietal cortices. Cognitive control errors were associated with decreased interactions at the cell level and with opposite changes at the network level in prefrontal and parietal cortices.

CONCLUSIONS: NMDAR synaptic deficits change causal interactions between neural signals at different levels of scale that correlate with schizophrenia-like deficits in cognitive control.

Keywords: AX-CPT, Causal modeling, Cognitive control, Neural dynamics, NMDA, Primate, Schizophrenia

https://doi.org/10.1016/j.bpsc.2020.02.013

Patients with schizophrenia (1–3) and other neuropsychiatric disorders (4–8) exhibit deficits in cognitive control, defined as the ability to use contextual information, such as goals and rules, stored in working memory to modify behavioral responses to environmental stimuli (9). This deficit has been measured using variants of the AX continuous performance task (AX-CPT) (3,7,10), in which a contextual cue (designated A or B) stored in working memory modifies the subsequent response to a probe stimulus (designated X or Y). Patients with schizophrenia (1,3), including those at first episode (11,12) as well as their first-degree relatives (13), exhibit robust deficits on the AX-CPT, suggesting that this task measures a specific deficit in cognition. Patients exhibit the most profound deficit when a B-cue stored in working memory countermands the habitual response to a subsequent X-probe (BX errors), a pattern of deficit observed to a lesser degree in other neuropsychiatric disorders, including depression (7,8) and bipolar disorder (4–6). To better understand the underlying defect in neural circuit operation that may contribute to this specific defect in cognitive control, we translated the dot pattern expectancy (DPX) task, a dot pattern variant of the AX-CPT, to nonhuman primates and conducted neural recording in prefrontal and posterior parietal cortex. We have shown previously that monkeys treated with an NMDA receptor (NMDAR) antagonist exhibit the same BX-selective error pattern (14) as patients with schizophrenia performing the DPX task (15). Here we contrasted neural dynamics in the prefrontal–parietal network under baseline conditions and following NMDAR blockade to understand how reduction of this synaptic mechanism disrupts neural circuit dynamics at the cellular, local circuit, and distributed network levels.

ISSN: 2451-9022

Cognitive control is thought to depend on goal or rule information that is represented in working memory by the persistent activation of subsets of prefrontal neurons selective for the items of stored information (9,16–20). The persistent activation of prefrontal neurons in turn is thought to depend on recurrent excitation in axon collateral networks that are particularly prominent in layer 3 (16,21,22) and particularly dependent on NMDAR synaptic currents. Pharmacological blockade of NMDAR but not AMPA receptor synaptic currents reduces persistent activity in prefrontal neurons of monkeys performing working memory tasks (23,24), and the sustained activity of neurons in artificial neural networks modeled on prefrontal cortex depends on NMDAR currents (25,26).

The above synaptic and circuit mechanisms of working memory in prefrontal cortex are selectively degraded in schizophrenia. Functional neuroimaging studies show reduced delay period prefrontal activation in patients performing working memory tasks (27), specifically on B-cue trials of the AX-CPT (1,11). NMDAR antagonists administered to healthy subjects replicate both hypofrontality and working memory deficits seen in schizophrenia (28,29), and a prominent cluster of schizophrenia risk mutations occur near genes with functional roles at NMDAR synapses (30–33). NMDARs are found on dendritic spines (34), which are reduced in density in schizophrenia, particularly in prefrontal cortex and particularly in layer 3 (21,35,36), where recurrent excitation in axon collateral networks is thought to contribute to persistent activity. These facts identify candidate neural circuit and synaptic mechanisms in prefrontal cortex, the disruption of which could contribute to working memory and cognitive control deficits in schizophrenia.

However, it is not known how biological events at the cell, synaptic, local circuit, and distributed network levels mutually influence each other to drive pathogenesis in schizophrenia or any other neuropsychiatric disease. There is as yet no ready way to measure the operation or functional state of individual neurons in the human brain of patients with neuropsychiatric disorders. To enable cell-level analysis of brain network failure during cognitive control deficits like those seen in schizophrenia, we have used a nonhuman primate model (14,18,37). Here we applied causal discovery analysis to time series of neural activity recorded at different levels of scale in prefrontal and parietal cortices to understand how physiological signals at the cellular, local circuit, and distributed network levels interact during cognitive control and how these interactions are disrupted by NMDAR synaptic malfunction.

METHODS AND MATERIALS

Behavioral Task

The behavioral and neural data we analyze in the current article were collected as part of our prior studies (18,37). Additional details regarding experimental methods can be found in those articles and in the current Supplement. Two male rhesus macaque monkeys performed the DPX task (Figure 1A–D). The DPX task is identical to the AX-CPT except that dot patterns replace letters as stimuli. Gaze angle was monitored using a video eye tracking system (Iscan, Woburn, MA), and monkeys maintained gaze fixated on a central target throughout each trial. Following 500 ms of initial fixation, a cue stimulus (1 second) was presented, followed by a delay period (1 second) and then a probe stimulus (0.5 second). Here 1 dot pattern constituted the A-cue, and 5 dot patterns collectively constituted B-cues. (Figure 1C). Similarly, 1 dot pattern constituted the X-probe, and 5 dot patterns collectively constituted Y-probes (Figure 1D). Monkeys moved a joystick to the left or right using their right hand following the onset of the probe. The rewarded joystick direction was a function of the cue–probe sequence. The AX cue–probe sequence was the target sequence and required a leftward movement (Figure 1A). All other cue–probe sequences were nontarget and required a rightward movement (e.g., BX sequence shown in Figure 1B). On the majority of trials (69%), the AX sequence was presented, establishing a prepotent tendency to produce the target (leftward) response to the X-probe. On the remaining 31% of trials, nontarget sequences were presented (12.5% AY, 12.5% BX, and 6% BY). Successful trials were rewarded with a drop of sweetened water. All animal care and experimental procedures conformed to National Institutes of Health guidelines and were approved by the Animal Care and Use Committee at the Minneapolis Veterans Administration Medical Center.

Neural Recording, NMDAR Antagonist Regimen, and Neural Database

We recorded 34 neuronal ensembles in the control condition (either with or without an injection of saline before first exposure to the NMDAR antagonist) and 34 neuronal ensembles in the drug condition (following injection of the NMDAR antagonist phencyclidine, 0.25–0.30 mg/kg intramuscular). We

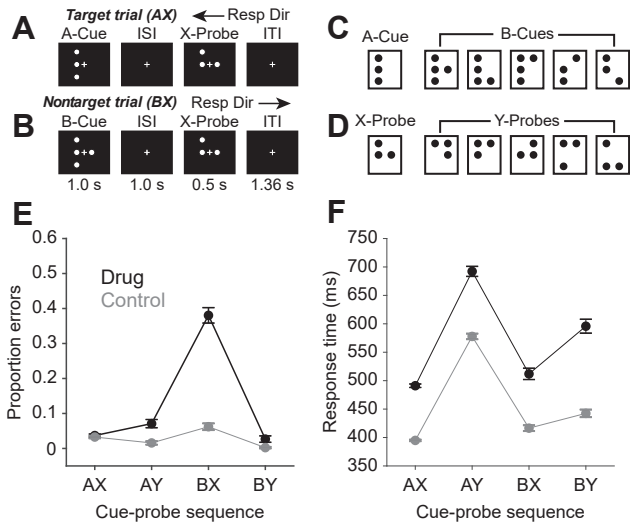

Figure 1. Dot pattern expectancy task and behavioral performance. **(A)** AX trial event sequence. The A-cue is followed by the X-probe, requiring a target response (left joystick movement). **(B)** BX trial event sequence. The B-cue is followed by the X-probe, requiring a nontarget response (right joystick movement). **(C)** Cue stimuli. **(D)** Probe stimuli. **(E)** Proportion of errors as a function of cue–probe sequence in the control condition (gray) and drug condition (black). **(F)** Response time as a function of cue–probe sequence in the control condition (gray) and the drug condition (black). Error bars in **(E, F)** represent twice the standard error of the mean. ISI, interstimulus interval; ITI, intertrial interval; Resp Dir, response direction.

restricted analyses to the subsets of neurons in prefrontal and parietal cortices that significantly modulated their firing in relation to task events (see Supplement). In total, we analyzed the spiking activity of 1762 cortical neurons. The 34 neuronal ensembles in the control condition included 289 task-related parietal neurons (average of 11 per ensemble) and 468 task-related prefrontal neurons (average of 15 per ensemble). The 34 neuronal ensembles in the drug condition included 434 task-related parietal neurons (average of 13 per ensemble) and 571 task-related prefrontal neurons (average of 14 per ensemble).

Format of Data for Causal Discovery Analysis

We performed a causal discovery analysis separately on each simultaneously recorded neuronal ensemble in the control and drug conditions. The data for each analysis consisted of time series of both neural and task data concatenated over trials (averages of 217 trials per set for the control condition and 235 trials per set for the drug condition). Each trial was represented by a set of binary time series (all values coded as 0 or 1) that represented the spiking of single neurons, modulations in local field potential (LFP) oscillatory power, and task state. Single neuron spiking data (2–32 neurons across ensembles) indicated whether or not an individual neuron generated an action potential in each 1-ms time bin. LFP data indicated whether oscillatory power fell above (1) or below (0) a threshold value in delta, theta, alpha, beta, and gamma bands (5 LFP variables per cortical area). The threshold was the 75th percentile of the distribution of values in each frequency band. We computed the time-varying power of LFP signals (1–100 Hz) using a Morlet wavelet analysis implemented using the ft_freqanalysis function in the FieldTrip MATLAB toolbox (MATLAB; The MathWorks, Inc., Natick, MA) (38). Time-frequency LFP data were calculated at a 1000-Hz resolution and then averaged across frequencies within frequency bands (delta: 1–4 Hz; theta: 4.1–8 Hz; alpha: 8.1–15 Hz; beta: 15.1–35 Hz; gamma: 35.1–100 Hz). LFP data were restricted to one channel selected at random in each cortical area to limit the total number of variables entered. Five task state variables were nonoverlapping step functions indicating whether the fixation, cue, delay, probe, and intertrial epoch were (1) or were not (0) currently active at each 1-ms time step. All data (single neuron, LFP, and task) were represented at 1000 Hz, beginning 499 ms before the onset of the cue stimulus and ending 1500 ms after the onset of the probe stimulus, for a total of 4000 data points per trial.

Causal Discovery Analysis

We used causal discovery (39,40) to estimate causal interactions between neural signals recorded at different levels of scale in the prefrontal–parietal network. We provide a conceptual description of the analysis here and provide additional details in the Supplement. Each experiment is represented as a set of nodes in a graph representing task state or neural signals recorded on a single electrode in prefrontal or parietal cortex. We used FGES (fast greedy equivalence search) (41), a causal discovery algorithm that finds the pattern of causal interactions between nodes (directed edges), represented as a Bayesian network, that simultaneously 1) maximizes the probability of the data given the model and 2) minimizes the number of edges. The probability of the data given the model is

$$P(X|M) = \Pi_{s\in S}\,\Pi_{v\in V}\,P_M\left(v = X_{s,v} \middle|\, M_{pa}(v) = X_{s,M_{pa}(v)}\right)$$

where X is the data, M is the model, and S and V are the samples and variables, respectively. P_M is a multinomial probability distribution computed from the data and stored as conditional probability tables in model M, $X_{s,v}$ is the value of variable v in sample s (0 or 1 in our case), $M_{pa}(v)$ is the set of variables that are "parents" of v (e.g., send directed edges to v) in model M, and $X_{s,M_{pa}(v)}$ is the corresponding set of values in those parent variables in sample s, The conditional probabilities between nodes are represented by directed edges in the graphs. This expression states that the conditional probability of the data X given model M is the product across connected nodes and samples of the conditional probabilities of the sample values. The conditional probabilities between the sample values defined by the pattern of connected nodes are computed directly from the data. In the example shown (Figure 2A), three nodes (two spike trains in individual neurons and one LFP power time series) are parents providing input to a fourth "child" node (neuron). The directed edges imply that the state of the parents at each time step (sample), represented as combinations of 0s and 1s (Figure 2B, left; [0,1,1; 1,0,1 ...]) influences the state of the child (Figure 2B, right; [0 or 1]). This influence is expressed as the conditional probability that the child (V_4) takes on a given value given the concurrent values of its three parents (V_1, V_2, V_3). At the first time step (S_1), the parents have values [0,1,1] and the child has value [0]. The conditional probability associated with this concurrent set of values in parents and child is $P(V_4 = 0 \mid V_1 = 0, V_2 = 1, V_3 = 1)$ (0.001 in this hypothetical example). That conditional probability is determined by counting the number of instances that this particular combination of values in parents and child

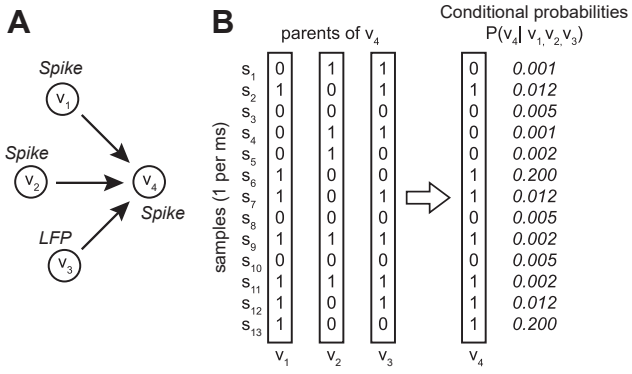

Figure 2. Conceptual schematic illustrating application of causal discovery analysis to neural time series data. **(A)** Graph showing directed edges from three parent nodes, V_1, V_2, and V_3 (two spiking neurons and one local field potential [LFP] power), to a child node, V_4 (spiking neuron). **(B)** Sequence of activity states (samples), each represented as a 0 or 1 at each time step, in the three parent nodes and the one child node along with the conditional probabilities associated with each combination of states at each time step. FGES (fast greedy equivalence search), a causal discovery algorithm, finds the pattern of edges that maximizes the product of the conditional probabilities over all samples and nodes in the network while minimizing the number of edges.

occurs divided by the total number of instances when the parents took on the values [0,1,1] regardless of the state of the child. The edges can be interpreted as causal in the sense that they indicate which nodes influence other nodes in terms of providing conditional probabilities included in the model. We evaluated conditional probabilities at 0-lag to measure synchronous neural interactions, analogous to the 0-lag spike correlation in prefrontal cortex we investigated previously (37). Consequently, the interactions we detected are likely mediated by reciprocal dynamics in polysynaptic networks that modulate synchrony at multiple levels of scale. We define microscale interactions as conditional probabilities between the spike trains (action potential time series) of individual neurons. We define mesoscale interactions as statistical dependencies between the spike trains of individual neurons and modulations in LFP power recorded in the same cortical area. We define macroscale interactions as statistical dependencies in neural signals (either spikes or LFPs) between cortical areas.

Quantification of Neural Interactions

We expressed the number of directed edges obtained in Bayesian networks as a proportion of the total possible number of edges given the number of variables entered, and we bias corrected these proportions by subtracting the number of edges that we could expect either at chance or to reflect entrainment of neural signals to external events (stimuli and responses) rather than real-time physiological interactions between neurons in circuits. For this purpose, we generated a permutation distribution of 100 Bayesian graphs for each neuronal ensemble after applying causal discovery analysis to trial-shuffled neural data (keeping the time series for each trial within each variable intact). This retained the entrainment of neural signals to external events but broke the simultaneity of the neural signals, precluding physiological interactions between neurons in circuits from contributing to the detected interactions. We then subtracted the mean of the number of directed edges in the permutation distribution from the number of directed edges in the original data. (See Figure S1 for an example of this correction procedure.) Differences in the proportion of bias-corrected directed edges in the Bayesian networks between the control and drug conditions in the original data were deemed significant if they exceeded the 95th percentile of 100 condition differences generated from the trial-shuffled data.

RESULTS

Behavioral Performance

In the baseline condition, the monkeys' performance on the DPX task (Figure 1A, B) was 97% correct, and the BX error rate was 8% (Figure 1E, gray). In the drug condition, the BX error rate increased to 38% (Figure 1E, black), and the proportion of errors was significantly greater on BX trials in comparison with the other trial types ($\chi^2_1 = 2218$, $n = 12{,}676$ trials, $p < .001$). BX trials impose high proactive cognitive control demand (12,42) because the B-cue stored in working memory must countermand the habitual target response to the subsequent X-probe. AY trials impose high reactive cognitive control demand because presentation of the Y-probe must countermand the habitual target response associated with the A-cue stored in working memory. AY trials were associated with elevated response time (RT) in both the drug condition (Figure 1F, black) and control condition (Fig. 1F, gray), perhaps reflecting elevated reactive control demand. In the drug condition, RTs significantly differed as a function of trial type (Figure 1F) (Kruskal–Wallis test, $\chi^2_{3,11488} = 2292$, $p < .001$), with RTs on AY trials being significantly greater than RTs on BY trials (Tukey honestly significant difference, $p < .05$). The similarity in RTs across trial types in the drug and control conditions (Figure 2F) suggests that monkeys applied similar cognitive strategies to task stimuli with and without NMDAR blockade. The difference in RT on AY versus BY trials in the drug condition provides evidence that monkeys continued to treat the task as a conditional response task following NMDAR blockade given that the cue (A-cue vs. B-cue) continued to influence processing time to respond to the probe (Y-probe).

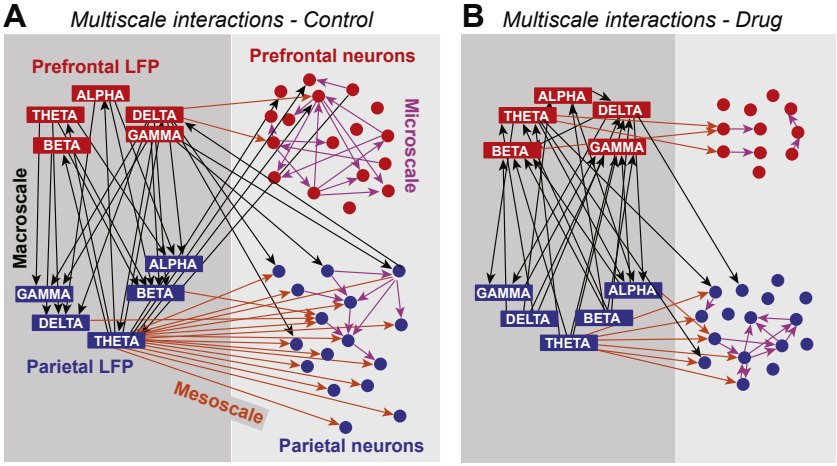

Figure 3. Example graphs illustrating the pattern of multiscale interactions detected in simultaneously recorded neural data. Causal discovery analysis was applied to time series of neural signals recorded simultaneously in prefrontal (red) and parietal (blue) cortex. Data are from examples of individual neural recording sessions. Thresholded local field potential (LFP) time series at each of five frequency bands are represented by boxes. Time series of spiking activity in individual neurons are represented by circles. Edges indicate detected interactions between neural signals. Color indicates the level of scale of the interaction: microscale (between spiking neurons; pink arrows), mesoscale (between spiking neurons and LFP signals in the same cortical area; orange arrows), or macroscale (between cortical areas, either spiking neurons or LFP signals: black arrows). **(A)** Example directed graph derived from an individual neural recording session under the control condition. **(B)** Example directed graph derived from a different individual neural recording session under the drug condition.

Causal Interactions Between Neural Signals

The results of the causal discovery analysis applied to our neural data described interactions at three levels of scale in the brain. Microscale interactions (Figure 3, pink arrows linking neurons, circles) were detected between the spike trains of simultaneously recorded neurons within the same cortical area, indicating the influence of spiking in one neuron on spiking in another neuron. Mesoscale interactions were detected between spike trains of neurons and simultaneously recorded LFP signals within the same cortical area (Figure 3, orange arrows). Mesoscale interactions captured the extent to which power fluctuations in oscillatory LFP components influenced single neuron spiking in local circuits. Macroscale interactions were detected between LFP signals (or LFP signals and neuronal spike trains) recorded simultaneously in different cortical areas (Figure 3, black arrows). Macroscale interactions captured neural dynamics across cortical areas communicating in distributed corticocortical networks.

Microscale (Cell–Cell) Interactions

We quantified microscale (cell–cell) interactions between the spike trains of neurons at the population level by counting the number of directed edges between neurons detected by causal discovery analysis in relation to the total number of edges possible in the data (constrained by the number of pairs of simultaneously recorded neurons). We found that systemically blocking NMDARs produced opposite effects on microscale (cell–cell) interactions in parietal and prefrontal local circuits, significantly enhancing these interactions in parietal cortex (Figure 4A) ($p < .01$, permutation test; see Methods and Materials) and suppressing them in prefrontal cortex (Figure 4B) ($p < .01$). The prefrontal finding is consistent with our prior report based on a different statistical analysis (37).

Mesoscale (Local Circuit–Cell) Interactions

In parietal cortex, mesoscale interactions between LFPs and neuronal spike trains were dominated by LFP oscillations in the theta band (4–8 Hz) relative to other frequencies (Figure 5A). In prefrontal cortex, the prominent peak of mesoscale interactions at theta frequencies was not evident (Figure 5B). NMDAR blockade significantly weakened theta band mesoscale interactions in parietal cortex and significantly enhanced them in prefrontal cortex (Figure 5A, B, red vs. blue) ($p < .01$). Collapsing across frequencies, mesoscale interactions were significantly weakened in both cortical areas, although only modestly in prefrontal cortex (Figure 5C, D).

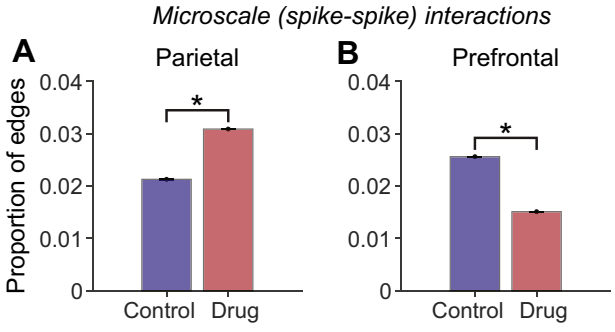

Figure 4. Influence of NMDA receptor blockade on microscale interactions. Data are permutation-corrected proportions of significant interactions between neurons relative to the total number of possible interactions given the number of neurons recorded. Blue: Control condition. Red: Drug condition. **(A)** Parietal neurons. **(B)** Prefrontal neurons. Error bars represent the standard deviation of the permutation distributions. Significant differences are indicated by asterisk (permutation test, $^*p < .01$).

Macroscale (Area–Area) Interactions

Blocking NMDARs significantly increased bottom-up (Figure 6A) and decreased top-down (Figure 6B) macroscale interactions between LFP signals in prefrontal and parietal cortices. Blocking NMDARs increased bottom-up (Figure 6C) and also top-down (Figure 6D) macroscale interactions between LFP signals in the theta band in one cortical area and spikes in the other. Collapsing across frequency bands, bottom-up macroscale interactions between LFP signals in parietal cortex and spikes in prefrontal cortex were significantly enhanced (Figure 6E).

Multiscale Interactions That Predict Failure in Cognitive Control

Both patients with schizophrenia (11,12) and monkeys administered NMDAR antagonists (14) (Figure 1E) performing the AX-CPT and DPX tasks exhibit a selective increase in errors on BX trials when a B-cue stored in working memory must countermand a habitual response to the X-probe. To isolate changes in network dynamics associated with the commission of BX errors, we stratified trials by cue–probe sequence and trial outcome and repeated the causal discovery analysis on the resulting subsets of trials (Figure 7). To understand how network dynamics change in response to increased cognitive control demand associated with the B-cue, we compared causal interactions on correct BX trials with interactions on AX trials. To understand how failure of network interactions leads to BX errors, we compared causal interactions on BX correct trials with interactions on BX error trials. We restricted this analysis to trials performed in the drug condition when there were enough errors to analyze (Figure 1E). As shown in Figure 7, in the drug condition, we found that microscale (spike–spike) interactions between neurons increased in both parietal cortex (Figure 7A) and prefrontal cortex (Figure 7B) on correct BX trials (light purple) relative to correct AX trials (orange) and further that these changes reversed when monkeys made BX errors (dark purple). We also found that in the drug condition, macroscale (LFP–LFP) parietal-to-prefrontal interactions increased (Figure 7E), whereas prefrontal-to-parietal interactions decreased (Figure 7F), on correct BX trials (light purple) relative to correct AX trials (orange). These changes in macroscale interactions on correct BX relative to AX trials (Figure 7E, F) were in the same direction as changes seen in the drug condition relative to the control condition overall (Figure 6A, B; collapsing across trial types). This suggests that perturbations in macroscale interactions in the drug condition relative to the control condition may have been pronounced on BX trials in the drug condition. The decrease in prefrontal-to-parietal macroscale interactions evident on BX correct trials reversed on BX error trials (Figure 7F). Mesoscale interactions exhibited a weaker relation to trial type and outcome

(Figure 7C, D). These data provide a dynamical signature of cognitive control failure in the form of altered neural interactions in the prefrontal–parietal network when monkeys made BX errors.

DISCUSSION

Schizophrenia is a complex disorder resulting from interactions among biological variables operating at different levels of scale in the brain. For example, risk mutations have been identified that alter cell-level variables such as the molecular mechanisms of synaptic transmission, synaptic plasticity, and electrical excitability in neurons (31–33,43). Other risk mutations alter circuit-level variables such as the pattern and density of axonal projections linking cells into neural circuits (44–46). These changes in neural function and circuit connectivity are likely to distort the physiological dynamics of neural circuits. Schizophrenia risk mutations engineered into animal models have been shown to distort attractor dynamics in visual cortex (47) and hippocampus (48) as well as oscillatory synchrony between prefrontal cortex and hippocampus (49). Because schizophrenia is likely to involve both cell- and circuit-level changes, it is important to understand how cell- and circuit-level variables interact during pathogenesis. Neurons adjust their electrical excitability and synaptic connectivity to other neurons in response to the spatial and temporal patterns of synaptic inputs they experience (50). Those changes in synaptic connectivity in turn modify patterns of network activity and therefore feed back to further modify synaptic inputs to neurons. A complex interplay between cell state and circuit activity therefore tunes neural networks as neurons adjust their intrinsic properties in response to electrical activity patterns. We recently proposed that schizophrenia may involve a

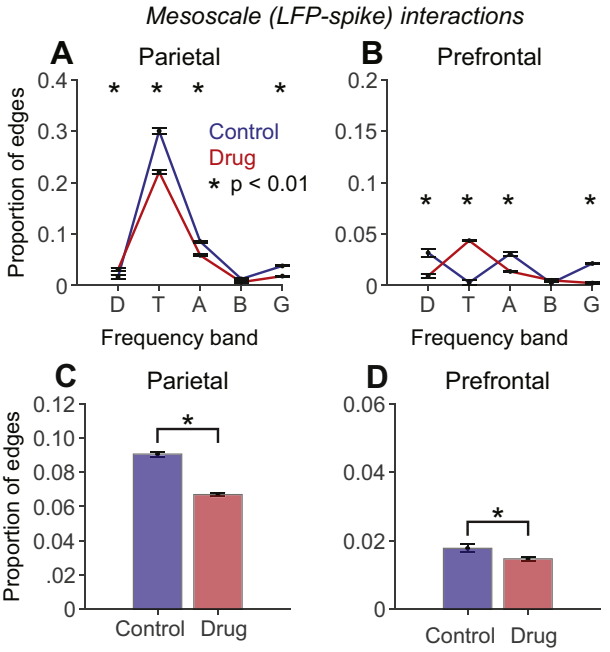

Figure 5. Influence of NMDA receptor blockade on mesoscale interactions. Data are permutation-corrected proportions of significant interactions between local field potential (LFP) signals and spike trains within the same cortical area relative to the total number possible given the number of paired LFP recordings, the number of frequency bands analyzed, and the number of recorded neurons. Blue: Control condition. Red: Drug condition. **(A, B)** Mesoscale interactions within parietal cortex **(A)** and prefrontal cortex **(B)** separated by LFP frequency band. Delta, theta, alpha, beta, and gamma bands are represented by D, T, A, B, and G, respectively. **(C, D)** Mesoscale interactions in parietal cortex **(C)** and prefrontal cortex **(D)** collapsed across frequency bands. Error bars represent the standard deviation of the permutation distributions. Significant differences are indicated by asterisk (permutation test, $p < .01$).

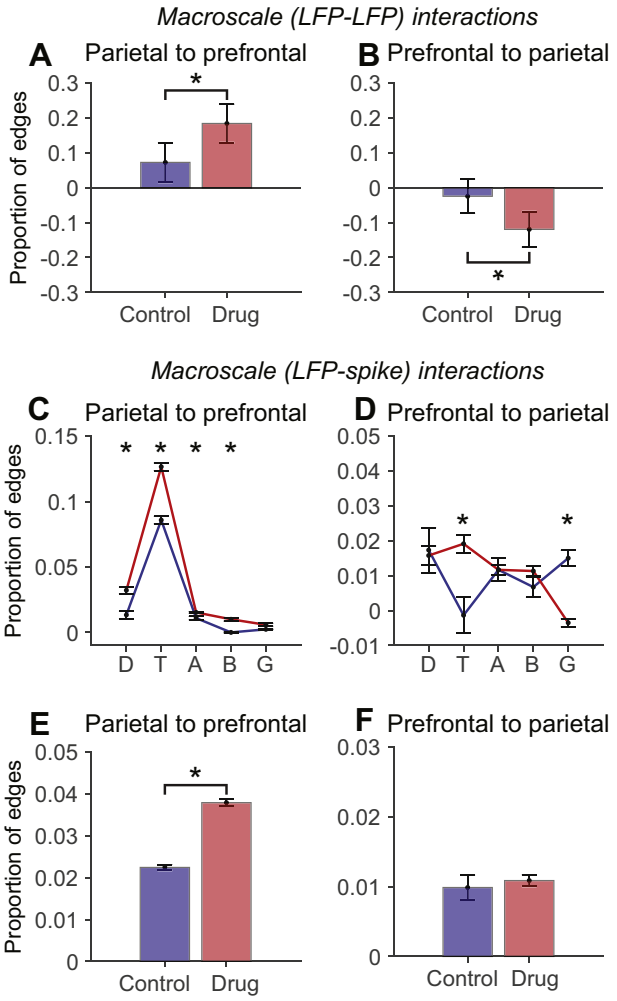

Figure 6. Influence of NMDA receptor blockade on macroscale interactions. Data are permutation-corrected proportions of interactions between local field potential (LFP) signals or between LFP signals and neuronal spike trains in prefrontal and parietal cortices relative to the total number possible given the number of LFP frequency bands and simultaneously recorded neurons. Blue: Control condition. Red: Drug condition. **(A, B)** Bottom-up **(A)** and top-down **(B)** macroscale (LFP–LFP) interactions. **(C, D)** Bottom-up **(C)** and top-down **(D)** macroscale (LFP–spike) interactions separated by frequency band. Delta, theta, alpha, beta, and gamma bands are represented by D, T, A, B, and G, respectively. **(E, F)** Bottom-up **(E)** and top-down **(F)** macroscale (LFP–spike) interactions collapsed across frequency bands. Error bars represent the standard deviation of the permutation distributions. Significant differences are indicated by asterisk (permutation test, $p < .01$).

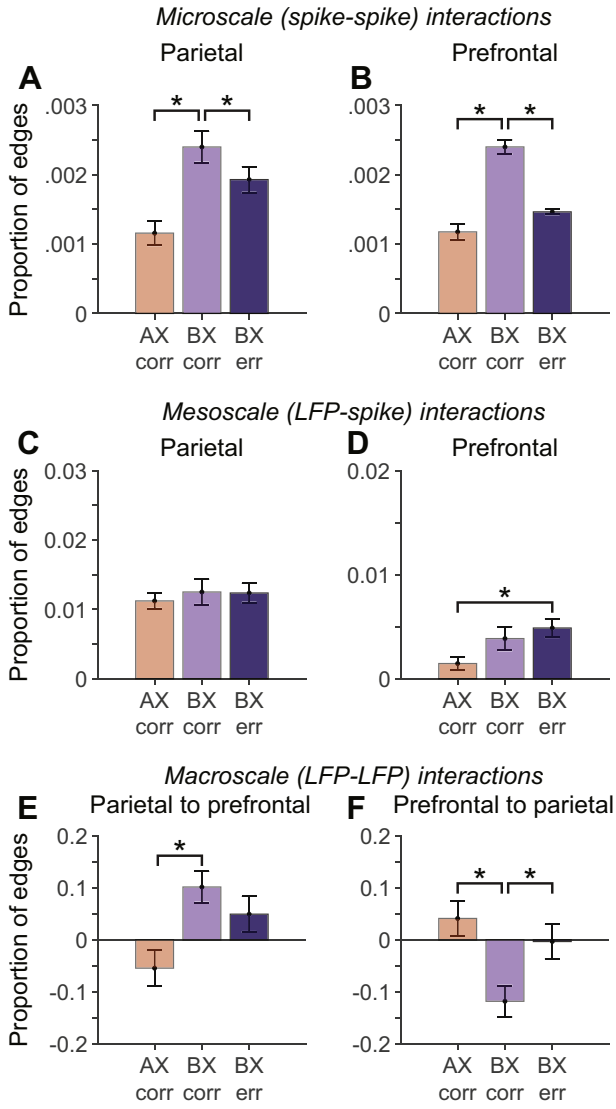

Figure 7. Relation of multiscale interactions to behavioral performance in the drug condition. Causal interactions are stratified by trial type (cue–probe sequence) and trial outcome (correct [corr] or error [err]). Data are permutation-corrected proportions of significant interactions between neural signals at different levels of scale relative to the total number possible on AX correct (orange), BX correct (light purple), and BX error (dark purple) trials. **(A, B)** Microscale (spike–spike) causal interactions in parietal cortex **(A)** and prefrontal cortex **(B)** as a function of trial type and outcome. **(C, D)** Mesoscale (LFP–spike) interactions within parietal cortex **(C)** and prefrontal cortex **(D)** as a function of trial type and outcome. **(E, F)** Macroscale (local field potential [LFP]–LFP) interactions in parietal cortex **(E)** and prefrontal cortex **(F)** as a function of trial type and outcome. Error bars represent the standard deviation of the permutation distributions. Significant differences are indicated by asterisk (permutation test, $p < .01$).

distortion of this feedback process, by which reduction in synchronous spiking between neurons at the circuit level and disconnection of synapses at the cell level may accelerate each other in a positive feedback loop driving a downward spiral that ultimately disconnects prefrontal networks via an activity-dependent process (37). This theory has much in common with other theories of schizophrenia pathogenesis that also involve feedback interactions between cell- and circuit-level variables as elaborated by other groups (51–53). To further explore the relationship between cell- and circuit-level variables, and to learn how their interaction might be distorted in schizophrenia, we applied causal discovery analysis to time series of neural activity recorded at the cell, local circuit, and distributed network levels in prefrontal and posterior parietal cortices of monkeys performing a cognitive control task that measures deficits in schizophrenia (7,14,18). This allowed us to investigate how interactions between neural events across levels of scale were distorted by NMDAR synaptic malfunction, a schizophrenia-relevant manipulation (30,31,54).

NMDARs are broadly distributed throughout the cerebral cortex (34,55). One might predict that brainwide blockade of NMDARs via systemic administration of antagonists would have a globally suppressive effect on neuronal excitability, producing comparable effects in prefrontal and parietal cortices. Instead, we found marked divergence in how prefrontal and parietal neurons, circuits, and networks responded to NMDAR blockade. In general, communication between prefrontal neurons and top-down prefrontal output was suppressed, whereas communication between parietal neurons and bottom-up parietal output was increased, following NMDAR blockade (Figures 4 and 6). This provides evidence that prefrontal and parietal local circuits are differentially dependent on NMDAR synaptic mechanisms and that global insult to NMDARs can produce circuit-specific effects on neural activity. NMDAR subunits (NR1, NR2A, and NR2B) are expressed by most prefrontal and parietal neurons, but their concentration is higher in prefrontal cortex (56,57). Layer 3 pyramidal neurons in prefrontal and parietal cortices differ substantially in morphology, physiological properties, and patterns of gene expression (58). In prefrontal cortex, layer 3 pyramidal neurons are more likely to exhibit a bursting response to input and have more highly branched basilar dendrites that exhibit a higher density of spines in comparison with layer 3 pyramidal neurons in parietal cortex (58). Cross-correlation analysis has indicated that coincident spiking is more prevalent between parietal neurons than between prefrontal neurons (59). These data suggest that there may be differences in synaptic and local circuit mechanisms within prefrontal and parietal cortices that contribute to the differences in NMDAR sensitivity we observed.

One important question of particular relevance to schizophrenia is the nature of the communication failure that occurs in prefrontal circuits and networks when monkeys make BX errors in the task, given that this is the dominant pattern seen in the performance of patients. We identified specific changes in both microscale (Figure 7A, B) and macroscale (Figure 7E, F) neural interactions associated with successful engagement of cognitive control on correctly performed BX trials that reversed on BX errors. These data provide a dynamical signature of neural interactions that can predict cognitive control failure following NMDAR synaptic malfunction on a trial-by-trial basis.

Systemic administration of NMDAR antagonists to monkeys weakens LFP beta oscillations that encode trial outcome (60) as well as patterns of neuronal activity (24) and spike-field coherence (61) that encode cognitive rules. Iontophoretic

application or systemic administration of NMDAR antagonists weakens the persistent activity of prefrontal neurons (23) but spares their postsaccadic responses (23), suggesting circuit-specific effects. Administration of NMDAR antagonists to healthy subjects reduces functional connectivity between prefrontal and posterior parietal cortex during working memory tasks (28) but increases functional connectivity in the resting state (62,63), suggesting state-specific effects. In rat prefrontal cortex, NMDAR blockade increases neuronal firing rate but decreases 0-lag spike synchronization (64), suggesting that NMDARs influence spike timing independent of spike rate, as we have observed (37) (Figure 4B).

Applying a combination of computational modeling and dynamic causal analysis to magnetoencephalography data, Shaw *et al.* (65) reported that persons with schizophrenia performing a visual discrimination task exhibit reductions in gamma power that are consistent with reduced inhibitory tone in cortical circuits. Applying dynamic causal modeling to functional magnetic resonance imaging data, Zhou *et al.* (66) reported reduced top-down drive from prefrontal cortex to parietal cortex as well as increased bottom-up drive from posterior cingulate cortex to prefrontal cortex, a pattern of results broadly consistent with our own data (Figure 6A, B). Rosch *et al.* (67) demonstrated that administration of NMDAR antagonists to healthy subjects disrupted causal interactions within prefrontal cortex, as we observed (Figure 4B).

Our data document distinctive changes, and in some cases opposite changes, in network dynamics within prefrontal and parietal cortices in response to systemic administration of NMDAR antagonists. These findings suggest that NMDAR synaptic mechanisms play circuit-specific roles in the two cortical areas. We found that causal interactions linked neural signals across the cellular, local circuit, and distributed network levels of scale, potentially making it possible to infer the state of neurons from the state of networks. We also found that the pattern of causal interactions across scales varied with cognitive control load and predicted cognitive control failure on a trial-by-trial basis following NMDAR blockade. These data open a cell- and circuit-level window into how prefrontal networks fail following NMDAR synaptic malfunction that could provide mechanistic insight into how prefrontal networks fail in schizophrenia.

ACKNOWLEDGMENTS AND DISCLOSURES

Support for this work was provided by the National Institutes of Health (Grant No. R01MH107491 [to MVC], Grant Nos. R01MH080318 and R01MH112688 [to ADR], Grant No. NCRR 1UL1TR002494-01 [to EK and SM], Grant Nos. T32 GM008244 and T32 HD007151 [to RKB], Grant No. F31MH109238 [to ALD], and Grant Nos. R01MH081051, R21MH110208-01A1, and R21MH110208-01A1 [to SV]); and by the University of Minnesota Wilfred Wetzel Graduate Fellowship (to RKB). This material is the result of work supported with resources and the use of facilities at the Minneapolis Veterans Administration Health Care System.

The contents do not represent the views of the U.S. Department of Veterans Affairs or the U.S. government. RKB's contribution to this article was from work she conducted as an M.D./Ph.D. student at the University of Minnesota and in her private capacity. The opinions expressed in this article are the author's own and do not reflect the views of the National Institutes of Health, the Department of Health and Human Services, or the U.S. government.

We thank Dean Evans for his lab and project management as well as for assistance with surgeries, animal care, and neural recordings; Dale Boeff for his assistance with neurophysiological recording system design and construction as well as for computer programming for signal processing and data analysis; and Sofia Sakellaridi for her assistance with neural recordings. We also thank the Center for Causal Discovery for developing and supporting the open source Tetrad software package.

SV is on the scientific advisory boards of Mindstrong, Verily, and Alkermes. She has served as a site principal investigator on a National Institute of Mental Health Small Business Innovation Research grant to Posit Science. All other authors report no biomedical financial interests or potential conflicts of interest.

ARTICLE INFORMATION

From the Institute for Health Informatics (EK, SM), Medical Scientist Training Program (RKB), Department of Neuroscience (RKB, ALD, ADR, MVC), and Department of Psychiatry (SV), University of Minnesota; Brain Sciences Center (RKB, ALD, MVC), Veterans Administration Medical Center; and Department of Biology (DAC), Augsburg University, Minneapolis, Minnesota.

RKB's current address is the National Institute of Mental Health, Bethesda, Maryland.

EK and SM contributed equally to this work as joint first authors.

DAC and MVC contributed equally to this work as joint senior authors.

Address correspondence to Matthew Chafee, Ph.D., Department of Neuroscience, University of Minnesota School of Medicine, Brain Sciences Center (11B), Minneapolis VA Medical Center, 1 Veterans Drive, Minneapolis, MN 55417; E-mail: chafe001@umn.edu.

Received Jan 24, 2020; revised and accepted Feb 28, 2020.

Supplementary material cited in this article is available online at https://doi.org/10.1016/j.bpsc.2020.02.013.

REFERENCES

1. Perlstein WM, Dixit NK, Carter CS, Noll DC, Cohen JD (2003): Prefrontal cortex dysfunction mediates deficits in working memory and prepotent responding in schizophrenia. Biol Psychiatry 53:25–38.
2. Ray KL, Lesh TA, Howell AM, Salo TP, Ragland JD, MacDonald AW, *et al.* (2017): Functional network changes and cognitive control in schizophrenia. NeuroImage Clin 15:161–170.
3. Barch DM, Carter CS, MacDonald AW III, Braver TS, Cohen JD (2003): Context-processing deficits in schizophrenia: Diagnostic specificity, 4-week course, and relationships to clinical symptoms. J Abnorm Psychol 112:132–143.
4. Smucny J, Lesh TA, Iosif A-M, Niendam TA, Tully LM, Carter CS (2018): Longitudinal stability of cognitive control in early psychosis: Nondegenerative deficits across diagnoses. J Abnorm Psychol 127:781–788.
5. Smucny J, Lesh TA, Newton K, Niendam TA, Ragland JD, Carter CS (2018): Levels of cognitive control: A functional magnetic resonance imaging-based test of an RDoC domain across bipolar disorder and schizophrenia. Neuropsychopharmacology 43:598–606.
6. Robinson LJ, Thompson JM, Gallagher P, Gray JM, Young AH, Ferrier IN (2013): Performance monitoring and executive control of attention in euthymic bipolar disorder: Employing the CPT-AX paradigm. Psychiatry Res 210:457–464.
7. MacDonald AW 3rd (2008): Building a clinically relevant cognitive task: Case study of the AX paradigm. Schizophr Bull 34:619–628.
8. Msetfi RM, Murphy RA, Kornbrot DE, Simpson J (2009): Impaired context maintenance in mild to moderately depressed students. Q J Exp Psychol 62:653–662.
9. Miller EK, Cohen JD (2001): An integrative theory of prefrontal cortex function. Annu Rev Neurosci 24:167–202.
10. Carter CS, Minzenberg M, West R, Macdonald A 3rd (2012): CNTRICS imaging biomarker selections: Executive control paradigms. Schizophr Bull 38:34–42.
11. MacDonald AW 3rd, Carter CS, Kerns JG, Ursu S, Barch DM, Holmes AJ, *et al.* (2005): Specificity of prefrontal dysfunction and context processing deficits to schizophrenia in never-medicated patients with first-episode psychosis. Am J Psychiatry 162:475–484.
12. Lesh TA, Westphal AJ, Niendam TA, Yoon JH, Minzenberg MJ, Ragland JD, *et al.* (2013): Proactive and reactive cognitive control and

dorsolateral prefrontal cortex dysfunction in first episode schizophrenia. NeuroImage Clin 2:590–599.
13. Snitz BE, Macdonald AW 3rd, Carter CS (2006): Cognitive deficits in unaffected first-degree relatives of schizophrenia patients: A meta-analytic review of putative endophenotypes. Schizophr Bull 32:179–194.
14. Blackman RK, Macdonald AW 3rd, Chafee MV (2013): Effects of ketamine on context-processing performance in monkeys: A new animal model of cognitive deficits in schizophrenia. Neuropsychopharmacology 38:2090–2100.
15. Jones JA, Sponheim SR, MacDonald AW 3rd (2010): The dot pattern expectancy task: Reliability and replication of deficits in schizophrenia. Psychol Assess 22:131–141.
16. Goldman-Rakic PS (1995): Cellular basis of working memory. Neuron 14:477–485.
17. Goldman-Rakic PS (1990): Cellular and circuit basis of working memory in prefrontal cortex of nonhuman primates. Prog Brain Res 85:325–335; discussion 335–336.
18. Blackman RK, Crowe DA, DeNicola AL, Sakellaridi S, MacDonald AW 3rd, Chafee MV (2016): Monkey prefrontal neurons reflect logical operations for cognitive control in a variant of the AX continuous performance task (AX-CPT). J Neurosci 36:4067–4079.
19. Crowe DA, Goodwin SJ, Blackman RK, Sakellaridi S, Sponheim SR, MacDonald AW 3rd, Chafee MV (2013): Prefrontal neurons transmit signals to parietal neurons that reflect executive control of cognition. Nat Neurosci 16:1484–1491.
20. Chafee MV, Goldman-Rakic PS (1998): Matching patterns of activity in primate prefrontal area 8a and parietal area 7ip neurons during a spatial working memory task. J Neurophysiol 79:2919–2940.
21. Hoftman GD, Datta D, Lewis DA (2017): Layer 3 excitatory and inhibitory circuitry in the prefrontal cortex: Developmental trajectories and alterations in schizophrenia. Biol Psychiatry 81:862–873.
22. González-Burgos G, Barrionuevo G, Lewis DA (2000): Horizontal synaptic connections in monkey prefrontal cortex: An in vitro electrophysiological study. Cereb Cortex 10:82–92.
23. Wang M, Yang Y, Wang C-J, Gamo NJ, Jin LE, Mazer JA, *et al.* (2013): NMDA receptors subserve persistent neuronal firing during working memory in dorsolateral prefrontal cortex. Neuron 77:736–749.
24. Ma L, Skoblenick K, Seamans JK, Everling S (2015): Ketamine-induced changes in the signal and noise of rule representation in working memory by lateral prefrontal neurons. J Neurosci 35:11612–11622.
25. Compte A, Brunel N, Goldman-Rakic PS, Wang XJ (2000): Synaptic mechanisms and network dynamics underlying spatial working memory in a cortical network model. Cereb Cortex 10:910–923.
26. Wang XJ (1999): Synaptic basis of cortical persistent activity: The importance of NMDA receptors to working memory. J Neurosci 19:9587–9603.
27. Driesen NR, Leung H-C, Calhoun VD, Constable RT, Gueorguieva R, Hoffman R, *et al.* (2008): Impairment of working memory maintenance and response in schizophrenia: Functional magnetic resonance imaging evidence. Biol Psychiatry 64:1026–1034.
28. Driesen NR, McCarthy G, Bhagwagar Z, Bloch MH, Calhoun VD, D'Souza DC, *et al.* (2013): The impact of NMDA receptor blockade on human working memory-related prefrontal function and connectivity. Neuropsychopharmacology 38:2613–2622.
29. Umbricht D, Schmid L, Koller R, Vollenweider FX, Hell D, Javitt DC (2000): Ketamine-induced deficits in auditory and visual context-dependent processing in healthy volunteers: Implications for models of cognitive deficits in schizophrenia. Arch Gen Psychiatry 57:1139–1147.
30. Timms AE, Dorschner MO, Wechsler J, Choi KY, Kirkwood R, Girirajan S, *et al.* (2013): Support for the N-methyl-D-aspartate receptor hypofunction hypothesis of schizophrenia from exome sequencing in multiplex families. JAMA Psychiatry 70:582–590.
31. Schizophrenia Working Group of the Psychiatric Genomics Consortium (2014): Biological insights from 108 schizophrenia-associated genetic loci. Nature 511:421–427.
32. Kirov G, Pocklington AJ, Holmans P, Ivanov D, Ikeda M, Ruderfer D, *et al.* (2012): De novo CNV analysis implicates specific abnormalities of postsynaptic signalling complexes in the pathogenesis of schizophrenia. Mol Psychiatry 17:142–153.
33. Fromer M, Pocklington AJ, Kavanagh DH, Williams HJ, Dwyer S, Gormley P, *et al.* (2014): De novo mutations in schizophrenia implicate synaptic networks. Nature 506:179–184.
34. Conti F, Barbaresi P, Melone M, Ducati A (1999): Neuronal and glial localization of NR1 and NR2A/B subunits of the NMDA receptor in the human cerebral cortex. Cereb Cortex 9:110–120.
35. Glantz LA, Lewis DA (2000): Decreased dendritic spine density on prefrontal cortical pyramidal neurons in schizophrenia. Arch Gen Psychiatry 57:65–73.
36. Kolluri N, Sun Z, Sampson AR, Lewis DA (2005): Lamina-specific reductions in dendritic spine density in the prefrontal cortex of subjects with schizophrenia. Am J Psychiatry 162:1200–1202.
37. Zick JL, Blackman RK, Crowe DA, Amirikian B, DeNicola AL, Netoff TI, Chafee MV (2018): Blocking NMDAR disrupts spike timing and decouples monkey prefrontal circuits: Implications for activity-dependent disconnection in schizophrenia. Neuron 98:1243–1255.e5.
38. Oostenveld R, Fries P, Maris E, Schoffelen J-M (2011): FieldTrip: Open source software for advanced analysis of MEG, EEG, and invasive electrophysiological data. Comput Intell Neurosci 2011:156869.
39. Spirtes P, Glymour CN, Scheines R, Heckerman D, Meek C, Cooper G, Richardson T (2000): Causation, Prediction, and Search. Cambridge, MA: MIT Press.
40. Pearl J (2009): Causality. New York: Cambridge University Press.
41. Ramsey J, Glymour M, Sanchez-Romero R, Glymour C (2017): A million variables and more: The fast greedy equivalence search algorithm for learning high-dimensional graphical causal models, with an application to functional magnetic resonance images. Int J Data Sci Anal 3:121–129.
42. Barch DM, Ceaser A (2012): Cognition in schizophrenia: Core psychological and neural mechanisms. Trends Cogn Sci 16:27–34.
43. Fénelon K, Mukai J, Xu B, Hsu P-K, Drew LJ, Karayiorgou M, *et al.* (2011): Deficiency of Dgcr8, a gene disrupted by the 22q11.2 microdeletion, results in altered short-term plasticity in the prefrontal cortex. Proc Natl Acad Sci U S A 108:4447–4452.
44. Sekar A, Bialas AR, de Rivera H, Davis A, Hammond TR, Kamitaki N, *et al.* (2016): Schizophrenia risk from complex variation of complement component 4. Nature 530:177–183.
45. Sellgren CM, Gracias J, Watmuff B, Biag JD, Thanos JM, Whittredge PB, *et al.* (2019): Increased synapse elimination by microglia in schizophrenia patient-derived models of synaptic pruning. Nat Neurosci 22:374–385.
46. Fernandez A, Meechan DW, Karpinski BA, Paronett EM, Bryan CA, Rutz HL, *et al.* (2019): Mitochondrial Dysfunction Leads to Cortical Under-Connectivity and Cognitive Impairment. Neuron 102:1127–1142.
47. Hamm JP, Peterka DS, Gogos JA, Yuste R (2017): Altered cortical ensembles in mouse models of schizophrenia. Neuron 94:153–167.e8.
48. Zaremba JD, Diamantopoulou A, Danielson NB, Grosmark AD, Kaifosh PW, Bowler JC, *et al.* (2017): Impaired hippocampal place cell dynamics in a mouse model of the 22q11.2 deletion. Nat Neurosci 20:1612–1623.
49. Sigurdsson T, Stark KL, Karayiorgou M, Gogos JA, Gordon JA (2010): Impaired hippocampal-prefrontal synchrony in a genetic mouse model of schizophrenia. Nature 464:763–767.
50. Dan Y, Poo MM (2006): Spike timing-dependent plasticity: From synapse to perception. Physiol Rev 86:1033–1048.
51. Krystal JH, Anticevic A, Yang GJ, Dragoi G, Driesen NR, Wang X-J, Murray JD (2017): Impaired tuning of neural ensembles and the pathophysiology of schizophrenia: A translational and computational neuroscience perspective. Biol Psychiatry 81:874–885.
52. Uhlhaas PJ, Singer W (2015): Oscillations and neuronal dynamics in schizophrenia: The search for basic symptoms and translational opportunities. Biol Psychiatry 77:1001–1009.
53. Stephan KE, Friston KJ, Frith CD (2009): Dysconnection in schizophrenia: From abnormal synaptic plasticity to failures of self-monitoring. Schizophr Bull 35:509–527.
54. Javitt DC, Zukin SR, Heresco-Levy U, Umbricht D (2012): Has an angel shown the way? Etiological and therapeutic implications of the PCP/NMDA model of schizophrenia. Schizophr Bull 38:958–966.

55. Huntley GW, Vickers JC, Janssen W, Brose N, Heinemann SF, Morrison JH (1994): Distribution and synaptic localization of immunocytochemically identified NMDA receptor subunit proteins in sensory-motor and visual cortices of monkey and human. J Neurosci 14:3603–3619.
56. Scherzer CR, Landwehrmeyer GB, Kerner JA, Counihan TJ, Kosinski CM, Standaert DG, *et al.* (1998): Expression of N-methyl-D-aspartate receptor subunit mRNAs in the human brain: Hippocampus and cortex. J Comp Neurol 390:75–90.
57. Akbarian S, Sucher NJ, Bradley D, Tafazzoli A, Trinh D, Hetrick WP, *et al.* (1996): Selective alterations in gene expression for NMDA receptor subunits in prefrontal cortex of schizophrenics. J Neurosci 16:19–30.
58. González-Burgos G, Miyamae T, Krimer Y, Gulchina Y, Pafundo DE, Krimer O, *et al.* (2019): Distinct properties of layer 3 pyramidal neurons from prefrontal and parietal areas of the monkey neocortex. J Neurosci 39:7277–7290.
59. Katsuki F, Qi X-L, Meyer T, Kostelic PM, Salinas E, Constantinidis C (2014): Differences in intrinsic functional organization between dorsolateral prefrontal and posterior parietal cortex. Cereb Cortex 24:2334–2349.
60. Skoblenick KJ, Womelsdorf T, Everling S (2016): Ketamine alters outcome-related local field potentials in monkey prefrontal cortex. Cereb Cortex 26:2743–2752.
61. Ma L, Skoblenick K, Johnston K, Everling S (2018): Ketamine alters lateral prefrontal oscillations in a rule-based working memory task. J Neurosci 38:2482–2494.
62. Grimm O, Gass N, Weber-Fahr W, Sartorius A, Schenker E, Spedding M, *et al.* (2015): Acute ketamine challenge increases resting state prefrontal-hippocampal connectivity in both humans and rats. Psychopharmacology 232:4231–4241.
63. Anticevic A, Corlett PR, Cole MW, Savic A, Gancsos M, Tang Y, *et al.* (2015): N-methyl-D-aspartate receptor antagonist effects on prefrontal cortical connectivity better model early than chronic schizophrenia. Biol Psychiatry 77:569–580.
64. Molina LA, Skelin I, Gruber AJ (2014): Acute NMDA receptor antagonism disrupts synchronization of action potential firing in rat prefrontal cortex. PLoS One 9:e85842.
65. Shaw AD, Knight L, Freeman TCA, Williams GM, Moran RJ, Friston KJ, *et al.* (2020): Oscillatory, Computational, and Behavioral Evidence for Impaired GABAergic Inhibition in Schizophrenia. Schizophr Bull 46:345–353.
66. Zhou Y, Zeidman P, Wu S, Razi A, Chen C, Yang L, *et al.* (2018): Altered intrinsic and extrinsic connectivity in schizophrenia. NeuroImage Clin 17:704–716.
67. Rosch RE, Auksztulewicz R, Leung PD, Friston KJ, Baldeweg T (2019): Selective prefrontal disinhibition in a roving auditory oddball paradigm under N-methyl-D-aspartate receptor blockade. Biol Psychiatry Cogn Neurosci Neuroimaging 4:140–150.